η^1- and η^2-Coordination in a (Phosphaalkene)platinum(0) Complex

Theodorus A. van der Knaap, Friedrich Bickelhaupt,* [1a] Johanna G. Kraaykamp,[1b] Gerard van Koten,[1b] Jan P. C. Bernards,[1c] Hommo T. Edzes,[1c] Wiebren S. Veeman,[1c] Engbert de Boer,[1c] and Evert Jan Baerends[1d]

Scheikundig Laboratorium, Vrije Universiteit, Amsterdam, Anorganisch Chemisch Laboratorium, Universiteit van Amsterdam, and Laboratorium voor Fysische Chemie, Katholieke Universiteit, Nijmegen, The Netherlands

Received June 18, 1984

The complex [mesityl(diphenylmethylene)phosphine]bis(triphenylphosphine)platinum(0) (1) can coordinate its ligand mesityl(diphenylmethylene)phosphine (2) in either the η^1-mode **1a** or the η^2-mode **1b**. Solid-state ^{31}P NMR spectroscopy has confirmed the η^1-mode in the crystalline state that has previously been determined by X-ray crystallography. A detailed investigation of the ^{31}P and ^{195}Pt NMR spectra in toluene-d_8 and of their temperature dependence revealed that the equilibrium **1b** $\rightleftharpoons$ **1a** is established in solution with $\Delta H = 4 \pm 1$ kcal·mol^{-1} and $\Delta S = 15 \pm 5$ cal·mol^{-1}·K^{-1}, which to our knowledge is the first case of a directly observable equilibrium between the two coordination modes. A detailed theoretical analysis by Hartree–Fock–Slater (LCAO-Xα) calculations on the model system $(PH_3)_2Pt{\cdot}HP{=}CH_2$ (3) shows, in qualitative agreement with the experimental results, that the η^2-coordination (**3b**) corresponds to the Dewar–Chatt–Duncanson model and is energetically favored over the η^1-coordination (**3a**) due to the stronger π-back-donation ($d_{xz} \rightarrow \pi^*$, 0.505 e in **3b**; $d_{xz} \rightarrow \pi^*$, 0.255 e in **3a**), even though σ-donation is weaker ($\pi \rightarrow 6a_1$, 0.21 e in **3b**; lone pair $\rightarrow 6a_1$, 0.28 e in **3a**). However, the differences are not large and may be overruled by nonbonded interactions when larger ligands are involved. Nevertheless, the experimental evidence proves that the calculated order $\eta^2 > \eta^1$ holds for the rather bulky ligand **2**.

In a recent communication,[2] we reported on the synthesis and structure of the (phosphaalkene)platinum(0) complex [mesityl(diphenylmethylene)phosphine]bis(triphenylphosphine)platinum(0) (**1**). This complex exhibited apparently contradictory properties: the X-ray crystal structure determination established unambiguously that the phosphaalkene **2** was σ- or η^1-coordinated via the phosphorus atom, while NMR spectra in solution showed dynamic behavior and were indicative or π- or η^2-coordination.[2] We now present evidence that proves the occurrence of η^2-coordination in solution and furthermore reveals the interesting phenomenon of a directly observable dynamic equilibrium between the η^1-isomer **1a** and the η^2-isomer **1b**. (Scheme I).

Scheme I

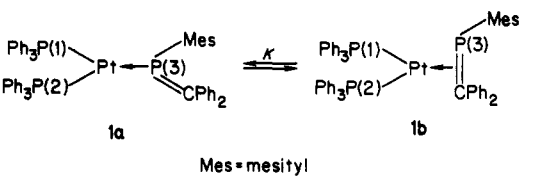

The Dynamic Equilibrium between 1a and 1b

Solid-State ^{31}P NMR Spectroscopy. Strong evidence in favor of η^2-coordination in solution had previously been derived from the unusual coordination chemical shift of P3 (vide infra); however, in view of the unprecedented structures involved, η^1-coordination with unusual bonding features could not be fully dismissed.[2] This latter possibility has now been excluded by solid-state ^{31}P NMR spectroscopy. The solid-state high-resolution ^{31}P NMR spectrum of **1a** is shown in Figures 1 and 2. The high-field part of the spectrum (Figure 1) shows two resonances at 50.0 and 40.5 ppm that are assigned to the phosphorus atoms P1 and P2 of the two triphenylphosphine ligands. Both resonances are accompanied by their ^1J(PtP) satellites. In contrast to the spectra obtained in solution at lower temperatures,[2] no signal is observed at the resonance positions for compound **1** in solution, i.e., around 22 and −30 ppm.

The resonance of P3 was more difficult to detect than those of the triphenylphosphine ligands. A large number of peaks with low intensity is observed in the low-field part of the spectrum (Figure 2). The complex pattern is due to the presence of a large chemical shielding anisotropy for P3, much larger than that for P1 and P2. In the absence of magic-angle spinning an extremely broad NMR line with a characteristic shape would result. Magic-angle spinning breaks up this pattern into a set of lines, consisting of a centerband and spinning sidebands for the P3 line and its ^1J(PtP3) satellites. The centerbands (Figure 2) are denoted by 0 and the spinning sidebands, at distances nf_R from the centerbands, by n and n'; f_R is the sample rotation frequency. Spinning sidebands are found also for P1 and P2 (Figure 1), but since the anisotropy of the chemical shielding is much smaller, just one sideband is observed. The position of the centerband, which is determined by the isotropic chemical shift, does not depend on the spinning frequency f_R. The isotropic shift of P3 was obtained from a comparison of spectra measured at two slightly different sample rotation rates (Figure 2) and is 247 ppm.

The total width of the spinning sideband pattern of P3 indicates that the chemical shielding anisotropy is large and spans about 350 ppm, the range over which the sidebands are observed. It would be of interest to obtain the principal elements of the chemical shielding tensor for ^{31}P in a P=C double bond. Procedures exist to derive these elements from the intensities of the spinning sidebands.[3,4] We have applied such an analysis[4] to the present data but were unable to obtain a satisfactory agreement

(1) (a) Vakgroep Organische Chemie, Vrije Universiteit, De Boelelaan 1083, 1081 HV Amsterdam. (b) Universiteit van Amsterdam. (c) Katholieke Universiteit, Nijmegen. (d) Afdeling Theoretische Chemie, Vrije Universiteit, Amsterdam.

(2) Van der Knaap, Th. A.; Bickelhaupt, F.; Van der Poel, H.; Van Koten, G.; Stam, C. H. *J. Am. Chem. Soc.* **1982**, *104*, 1756.

(3) Maricq, M. M.; Waugh, J. S. *J. Chem. Phys.* **1979**, *70*, 3300.

(4) Herzfeld, J.; Berger, A. E. *J. Chem. Phys.* **1980**, *73*, 6021.

0276-7333/84/2303-1804$01.50/0

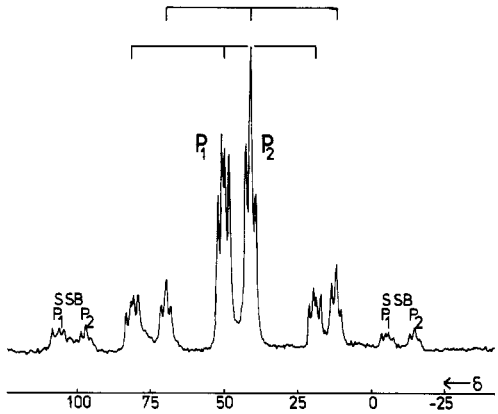

Figure 1. High-field part of the solid-state ^{31}P MAS NMR spectrum of **1a** (spinning frequency 4.1 kHz; δ in ppm). The ^1J(PtP) satellites of P1 and P2 are indicated by bars above the spectrum. SSB marks spinning side bands.

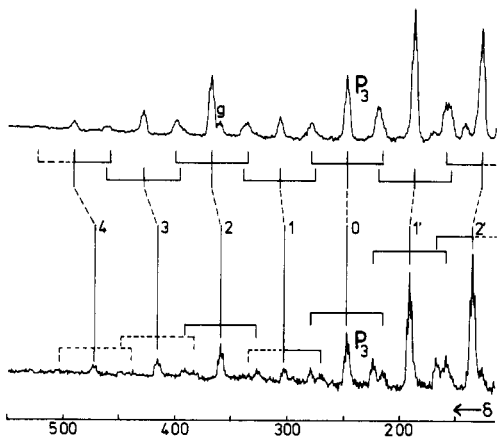

Figure 2. Low-field part of the solid-state ^{31}P MAS NMR spectrum of Figure 1. Upper trace: spinning frequency 4.4 kHz; lower trace: 4.1 kHz (δ in ppm). The order of the spinning side bands of P3 is indicated by numbers 1, 2, 3, 4, 1', and 2'. The corresponding ^1J(PtP3) satellites are indicated by bars. *g* is an artifact in the spectrum.

between theory and experiment. We ascribe this negative result to the simultaneous effect of P–P dipolar couplings and the chemical shielding anisotropy; in the theoretical analyses[3,4] only the latter interaction is taken into account. The simultaneous presence of the dipolar interaction and the anisotropic chemical shielding is known to distort the NMR line shapes considerably.[3,5]

The solid-state ^{31}P NMR data are summarized in Table I. They are in good agreement with expectation for η^1-coordination (**1a**); in particular, the low-field shift of P3 is close to that in the free ligand **2** itself (δ 233[6]), confirming the small coordination chemical shifts observed previously for η^1-coordinated phosphaalkenes.[7] Typical is also the large value of ^1J(PtP3) (4720 Hz); it is larger than ^1J(PtP1) and ^1J(PtP2) because the lone pair of ligand **2** has more s character than those of the triphenylphosphine ligands.

The ^{31}P parameters of the triphenylphosphine ligands are normal. Noteworthy is the nonequivalence of P1 and P2. It is caused by the rigid, unsymmetrical conformation of **1a** in the crystal: the angle between the σ plane of ligand

Table I. ^{31}P NMR Spectra of 1

		δ^a	^1J(PtP)^b	^2J(PP)^b	
1a[c]	P1	50.0	4560	P1P2	130
	P2	40.5	4260	P2P3	110
	P3	247	4720	P3P1	180
1a[d]	P1	48.0	4350	P1P2	
	P2	48.0	4350	P2P3	156
	P3	247.5	4960	P3P1	156
1b[d]	P1	25.0	3367	P1P2	31
	P2	22.4	3403	P2P3	10
	P3	−30.3	500	P3P1	56

[a] In ppm relative to external 85% H_3PO_4. [b] In hertz. [c] Solid state, 25 °C, 72.87 MHz. [d] Toluene-d_8, −70 °C, 101.26 MHz. For the temperature dependence of the ratio **1a**:**1b**, see Table III.

2 and that of PtP1P2 is fixed at 67°.[2] However, in solution, P1 and P2 of **1a** become equivalent (vide infra). The assignment of the chemical shifts, i.e., δ(P1) 50.0 and δ(P2) 40.5, is based on the rule that trans couplings ^2J(PMP') are generally larger than cis couplings.[7c,8] With the reservation that this rule has not been documented for tricoordinate platinum(0) and that the difference are small, application to **1a** would imply that the larger angle (P1PtP3 = 120.6 ± 0.1°)[2] is correlated with the larger ^2J(PP) = 180 Hz and the angle P2PtP3 (117.3 ± 0.1°) with ^2J(PP) = 110 Hz. However, this assignment must be considered as tentative.

We may conclude that the ^{31}P NMR spectrum and the X-ray structure determination both identify crystalline **1** as the η^1-complex **1a**. Consequently, the previously observed solution spectrum of **1**[2] must be assigned to the η^2-isomer **1b**. This assignment is consistent with the unusually large coordination shift of P3 ($\Delta\delta$ = 266 ppm) and the small ^1J(PtP3) (500 Hz).[2] Both changes are expected for η^2-coordination because the electron density at P3 is raised by π-back-donation from the metal to phosphorus, and there is little s contribution to the bonding between platinum and phosphorus. Analogous effects are well-known for the olefinic carbons of Pt(0)–alkene complexes;[9] they have recently also been observed for η^2-complexes of phosphaalkenes with Pt(0)[10] and Ni(0).[11]

Solution Spectroscopy. As pointed out previously,[2] the ^{31}P NMR spectra of **1** in toluene-d_8 are complicated by dynamic phenomena. Above −40 °C, the signals broaden; around room temperature, they gradually disappear without coalescence up to 100 °C. After the identification and assignment of the ^{31}P NMR parameters of **1a** in the solid state and of **1b** in solution, a reinvestigation of the solution spectra revealed that **1a** was also present in solution. The data of **1a** in solution and in the crystal are very similar (Table I). The most conspicuous difference is the equivalence of P1 and P2 in solution; at present, we cannot decide whether this is due to perpendicular orientation of the σ-plane of ligand **2** relative to the platinum coordination plane or to dynamic effects such as rapid oscillation or rotation around the PtP3 bond. In

(5) Zilm, K. W.; Grant, D. M. *J. Am. Chem. Soc.* **1981**, *103*, 2913.
(6) Klebach, Th. C.; Lourens, R.; Bickelhaupt, F. *J. Am. Chem. Soc.* **1978**, *100*, 4886.
(7) (a) Klebach, Th. C.; Lourens, R.; Bickelhaupt, F.; Stam, C. H.; Van Herk, A. *J. Organomet. Chem.* **1981**, *210*, 211. (b) Estiagh-Hosseini, H.; Kroto, H. W.; Nixon, J. F.; Maah, M. J.; Taylor, M. J. *J. Chem. Soc., Chem. Commun.* **1981**, 199. (c) Kroto, H. W.; Nixon, J. F.; Taylor, M. J.; Frew, A. A.; Muir, K. W. *Polyhedron* **1982**, *1*, 89.
(8) (a) Nixon, F. J.; Pidcock, A. *Annu. Rev. NMR Spectrosc.* **1969**, *2*, 345. (b) Allen, F. H.; Pidcock, A.; Waterhouse, C. R. *J. Chem. Soc. A* **1970**, 2087.
(9) (a) Chisholm, M. H.; Clarke, H. C.; Manzer, L. E.; Stothers, J. B. *J. Am. Chem. Soc.* **1972**, *94*, 5087. (b) Harrison, N. C.; Murray, M.; Spencer, J. L.; Stone, F. G. A. *J. Chem. Soc., Dalton Trans* **1978**, 1337.
(10) Al-Resayes, S. I.; Klein, S. I.; Kroto, H. W.; Meidine, M. F.; Nixon, J. F. *J. Chem. Soc., Chem. Commun.* **1983**, 930.
(11) (a) Cowley, A. H.; Jones, R. A.; Stewart, C. A.; Stuart, A. L.; Atwood, J. L.; Hunter, W. E.; Zhang, H. M. *J. Am. Chem. Soc.* **1983**, *105*, 3737. (b) Van der Knaap, Th. A.; Jenneskens, L. W.; Meeuwissen, H. J.; Bickelhaupt, F.; Walther, D.; Dinjus, E.; Uhlig, E.; Spek, A. L. *J. Organomet. Chem.* **1983**, *254*, C33.

Table II. ^{195}Pt NMR Spectra of 1 (53.68 MHz)

		^1J(PtP)[b]		
	δ[a]	P1	P2	P3
1a	−4410	4360	4360	4940
1b	−4847	3380	3380	500

[a] In ppm relative to external K_2PtCl_6 (0.5 M in D_2O); toluene-d_8; −40 °C. [b] In hertz.

Table III. Equilibrium Composition of 1a ⇆ 1b (Toluene-d_8) As Determined by NMR Spectroscopy

	^{31}P NMR		^{195}Pt NMR	
T, K	1a, %	1b, %	1a, %	1b, %
37			76	24
21			64	36
5	60	40		
−10	46	54	39	61
−25	37	63		
−40	26	74	20	80
−55	19	81		
−70	11	89		

this connection, it is of interest to point out that inspite of the smaller difference of the chemical shifts between P1 and P2 in **1b** (25.0 and 22.4 ppm, respectively) compared to **1a** (solid state, 50.0 and 40.5 ppm, respectively), they are nonequivalent when those of **1a** (solution) are not. This points to a considerable barrier of rotation of ligand **2** in the η^2-coordination mode. A closer inspection of Table I shows that the ^{31}P NMR parameters (δ, ^1J(PtP), ^2J(PP)) of **1a** in solution stay within the range given by the values in the solid state, but they are not the arithmetic means; an interpretation of the differences would be tempting but too speculative at this stage.

An investigation of the temperature dependence of the ^{31}P NMR spectra revealed that **1a** and **1b** are involved in a dynamic equilibrium; **1b** is the major isomer, but at higher temperature, the equilibrium shifts toward increasing amounts of **1a**. The two structural isomers could even more clearly be discerned in the ^{195}Pt NMR spectra (Table II), which do not suffer from dynamic phenomena because the chemical shift differences are much larger. By integration of the ^{195}Pt and the ^{31}P signals at different temperatures the equilibrium composition could be determined (Table III). The integrations are not very accurate, because the ^{31}P NMR spectra suffer from line broadening at higher temperatures, while the ^{195}Pt NMR spectra are difficult to integrate as the base line was curved due to the fast pulse technique employed for ^{195}Pt. However, within the limits of accuracy, the values for the thermodynamic parameters of the equilibrium **1b** ⇌ **1a** were equal and found to be $\Delta H = 4 \pm 1$ kcal·mol^{-1} and $\Delta S = 15 \pm 5$ cal·mol^{-1}·K^{-1}. The π-complex **1b** is favored at low temperature by its lower enthalpy, but the difference is small; at higher temperatures, the more positive entropy favors the σ-complex **1a**. The entropy difference may be related to a more rigid orientation of ligand **2** in the η^2-mode (vide supra).

Theoretical Analysis. In order to obtain some insight into the electronic and steric factors governing the coordination of phosphaalkenes, a theoretical study has been performed. We have used the Hartree–Fock–Slater (LCAO-Xα) method,[12] which differs from the Hartree–Fock method in the use of Slater's $\rho^{1/3}$ or Xα exchange potential instead of the full Hartree–Fock exchange operator. The method uses a frozen core and an expansion of the valence molecular orbitals (MO's) in Slater-type orbitals (STO's) as well as an auxiliary basis of density-fitting functions and special numerical integration techniques to evaluate the Fock matrix. The computational scheme affords an essentially ab initio calculation of the wave function, the quality of which thus depends on the HFS model and the size of the basis set. We have chosen a fairly flexible basis set of double-ζ quality, including the Pt 6p AO, with the addition of a 3d polarization function on P. In order to keep the calculations tractable, the model fragments $Pt(PH_3)_2$ and $HP{=}CH_2$ have been used. This implies that the results have qualitative rather than quantitative significance. The geometries have been chosen in accordance with X-ray structural data on **1a**.[2,13]

The relevant geometrical parameters are indicated in **3a** and **3b**. Structure **3a** presents the η^1-coordination with $HP{=}CH_2$ lying in the PPtP plane of the $Pt(PH_3)_2$ fragment. As this is our xz plane (note the choice of axes in (**3a** and **3b**), we denote this coordination as η^1_{xz}. The

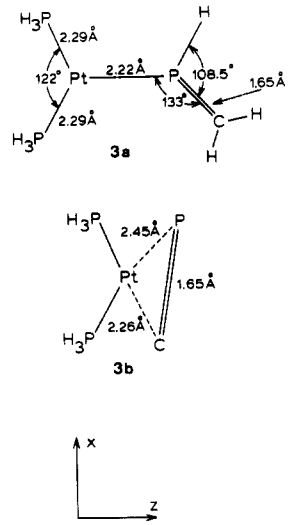

$HP{=}CH_2$ ligand may be rotated around the Pt–P axis to the yz plane; this structure will be denoted as the η^1_{yz}-coordination. For the η^2-coordination (**3b**), structural data are not available. We have oriented the plane of the $HP{=}CH_2$ ligand perpendicular to the xz plane, but not completely parallel to the xy plane, as the P=C bond is unsymmetrical. In order to maximize orbital interactions with $Pt(PH_3)_2$, the P=C bond axis has been slightly rotated to bring C somewhat closer to Pt compared to P (Pt–C = 2.264 Å; Pt–P = 2.449 Å); in this orientation, Pt lies in the nodal plane of the $HP{=}CH_2$ π^* orbital (vide infra). We only use the η^2_{xz}-coordination with P–C in the xz plane, as this is probably the preferred coordination for the same reason as it is for ethylene (vide infra).

It is possible to break up the total interaction energy between the molecular fragments into a steric contribution and charge transfer + polarization terms (so-called

(12) (a) Baerends, E. J.; Ellis, D. E.; Ros, P. *Chem. Phys.* **1973**, *2*, 41. (b) Baerends, E. J.; Ros, P. *Int. J. Quantum Chem.* **1978**, *S12*, 169.

(13) The structural data of the model ligand $HP{=}CH_2$ are thus slightly different from those used in our previous calculations of the free ligand.[14] Therefore, the computational results are quantitatively slightly different from the previous ones, but the qualitative conclusions are unchanged. Also it should be pointed out again[14] that the geometry of $HP{=}CH_2$ used in our calculations is not the experimentally determined one of the "real" molecule[15] but rather that of **2**, because this gives a better approximation of the bonding situation of **2**.[14]

(14) Van der Knaap, Th. A.; Klebach, Th. C.; Visser, F.; Bickelhaupt, F.; Ros, P.; Baerends, E. J.; Stam, C. H.; Konijn, M. *Tetrahedron* **1984**, *40*, 765.

(15) (a) Kroto, H. W.; Nixon, J. F.; Ohne, K. *J. Mol. Spectrosc.* **1981**, *90*, 367. (b) Brown, R. D.; Godfrey, P. D.; McNaughton, D. *Aust. J. Chem.* **1981**, *34*, 465.

"electronic interaction terms").[16] The steric contribution includes the electrostatic interaction between the nuclei and electronic charge densities of the original fragments put at the relative positions they have in the final complex plus overlap repulsion between the occupied orbitals of the two fragments. The electronic interaction terms are charge-transfer (HOMO–LUMO) type of interactions plus polarization of the fragments. It is possible, using the transition-state method of Ziegler,[17] to evaluate the electronic interaction terms separately for each irreducible representation. This allows in favorable cases a quantitative measure of the relative strength of, e.g., σ and π bonds. This method has been used by Ziegler and Rauk[16b] in an investigation of the Dewar–Chatt–Duncanson (DCD) coordination of ethylene to $Pt(Cl_3)^-$ (Zeise's salt) and to $Pt(PH_3)_2$. A related ab initio study, using a slightly different decomposition of the interaction energy, is that of Kitaura et al. on the bonding of C_2H_4 and C_2H_2 to $Ni(PH_3)_2$.[18] Also relevant is the study by Albright, Hoffman, and co-workers on rotational barriers in ethylene complexes.[19] The interesting feature of $HP{=}CH_2$ is that it not only has a P=C double bond, with which it presumably can coordinate in a DCD synergistic bonding mode to a transition metal, but also a lone pair at P, with which it can form a donative σ-coordination bond. In Figure 3 we give level ordering diagrams of the one-electron energies of $HP{=}CH_2$ and $Pt(PH_3)_2$ obtained in HFS calculations and also include a number of contour plots of frontier orbitals of the fragments in the xz and yz planes. It is to be noted that HFS one-electron energies do not correspond to ionization potentials (as in Hartree–Fock within the frozen orbital (Koopman's) approximation). They show, however, an almost uniform shift with respect to the computed ionization potentials. The differences in orbital energies may be used qualitatively as a measure of the energy denominator in the second-order expression for the stabilization due to orbital interaction, $H^2_{ij}/\Delta E$. The interaction matrix element H_{ij} between fragment orbitals ϕ_i and ϕ_j is approximately proportional to their overlap. It is possible to obtain a qualitative impression of the relative magnitudes of these overlaps from the contour plots of the valence orbitals of $HP{=}CH_2$ and $Pt(PH_3)_2$ in Figure 3. We will first discuss briefly the electronic structure of the two fragments using the data in Figure 3.

Starting with $Pt(PH_3)_2$ we note that the $(PH_3)_2$ ligands induce an important splitting and hybridization within the (occupied) 5d manifold. In particular, there is a notable difference between the d_{xz} and d_{yz} orbitals, which are responsible for π-back-bonding. The d_{xz} has an antibonding admixture of the PH_3 σ (lone pair) orbitals, which pushes it ca. 1.5 eV above d_{yz}. It also mixes in $6p_x$ character to diminish the antibonding, which results in considerable spatial extent of this orbital at the side of the incoming $HP{=}CH_2$ ligand. It is clear that $4b_1$ (d_{xz}) is much more suitable for π-bonding than is $2b_2$ (d_{yz}). This in fact accounts for the preference of ethylene to coordinate to $Pt(PH_3)_2$ in the PPtP plane rather than in the perpendicular geometry.[16b] When considering π-interactions of the $Pt(PH_3)_2$ fragment with $HP{=}CH_2$, we will have to keep in mind this difference between d_{xz} and d_{yz}. The d orbitals of A_1 symmetry $4a_1$ (mainly d_{z^2}) and $5a_1$ (mainly $d_{x^2-y^2}$) show less mixing with the PH_3 ligands. The $d_{x^2-y^2}$ is higher in energy due to antibonding interaction with the lone pairs of the PH_3 ligands. The d_{z^2} is strongly directed toward $HP{=}CH_2$, so it may both have considerable overlap repulsion with occupied orbitals of $HP{=}CH_2$ and act as a σ-donor toward $HP{=}CH_2$, depending on the frontier orbitals available. The $d_{x^2-y^2}$ orbital has its main amplitude in the xy plane, perpendicular to the Pt—P bond, and is expected to be less important for the coordination of $HP{=}CH_2$. The d_{xy} ($2a_2$, not plotted) is probably not involved at all. The LUMO of $Pt(PH_3)_2$ ($6a_1$) is a dsp hybrid directed toward $HP{=}CH_2$ and ideally suited for interaction with a σ donor orbital on the ligand.

Turning next to $HP{=}CH_2$, we first of all observe that the lone-pair orbital (5a′) has the expected characteristic of large amplitude at P and rotational symmetry around the Pt—P axis. It is evident from the plots that the experimental Pt–P–C angle in **3a** is such as to maximize the overlap of 5a′ with the σ-acceptor $6a_1$ of $Pt(PH_3)_2$. It is clear that this HOMO–LUMO interaction would allow almost free rotation around the Pt–P axis. There is also a σ-bond in η^2-coordination (**3b**), by σ-donation from the $HP{=}CH_2$ π-orbital (1a″) to the $Pt(PH_3)_2$ $6a_1$ LUMO, probably again without much difference in energy between the in-plane (i.e., η^2_{xz}) and perpendicular (η^2_{yz}) orientation.

As for π-type interactions, we wish to emphasize that these are present both in the η^2 (Dewar–Chatt–Duncanson) coordination (**3b**) and in the η^1-coordination (**3a**). This is evident for the η^2-coordination from the plot of 2a″ (π^*) in the xz plane. The d_{xz} orbital will cause preferential orientation of the P=C unit of **3b** in the xz plane; note that the P=C bond has been oriented such that Pt lies in the nodal plane of π^* in order to maximize the d_{xz}–π^* interaction. For the η^1-coordination (**3a**), there is also the possibility of π-back-bonding, in a manner reminiscent of the interaction with the CO π^*-orbital in carbonyl complexes. This is illustrated in the plot in the yz plane of the π^* orbital of the η^1_{xz}-coordinated $HP{=}CH_2$. It is clear that for this geometry $d_{yz} \rightarrow \pi^*$ back-bonding may occur. If η^1-coordinated $HP{=}CH_2$ is rotated around the Pt–P axis to the yz plane, the π-back-bonding will be $d_{xz} \rightarrow \pi^*$. This is expected to be stronger than $d_{yz} \rightarrow \pi^*$, so the π-bond may now induce a conformational preference of η^1-$HP{=}CH_2$ for the yz plane (note that for the same reason it directs η^2-$HP{=}CH_2$ to lie in the xz (PPtP) plane). For the sake of completeness we finally consider the LUMO of $HP{=}CH_2$ in the A′ symmetry, the 6a′ (σ^*) orbital. The contour plot shows that this orbital may act as a π-acceptor in the η^1-coordination, in as much as its high energy will allow it.

It is clear from this discussion that it is not a simple matter to establish the preferred coordination mode of $HP{=}CH_2$ to $Pt(PH_3)_2$. In all cases both σ- and π-interactions are possible, so it depends on the relative abilities of the P lone pair and P=C π-orbitals to act as a σ-donor and of the π^* in either η^1 or η^2 (DCD) mode to act as a π-acceptor, which one of the possibilities will prove energetically more favorable. We will examine the results of the SCF calculations to get a feeling for the relative importance of the various interactions. In Table IV, the orbital energies are given of the valence orbitals of both fragments, as well as the Mulliken gross orbital populations. In Table V, a number of relevant overlaps are given, being a measure for the strength of interactions. Table VI contains energy terms, which for the η^1-coordination geometries are separated in the A′ and A″ symmetries of the C_s symmetry that holds in both cases. In the η^2_{xz}-coordination, there is no symmetry left. We present the

(16) (a) Kitaura, K.; Morokuma, K. *Int. J. Quantum Chem.* **1976**, *10*, 325. (b) Ziegler, T.; Rauk, A. *Inorg. Chem.* **1979**, *18*, 1558. (c) Whangbo, M. H.; Schlegel, H. B.; Wolfe, S. *J. Am. Chem. Soc.* **1977**, *99*, 1296.
(17) Ziegler, T.; Rauk, A. *Theor. Chim. Acta* **1977**, *46*, 1.
(18) Kitaura, K.; Sakaki, S.; Morokuma, K. *Inorg. Chem.* **1981**, *20*, 2292.
(19) Albright, T. A.; Hoffmann, R.; Thibeault, J. C.; Thorn, D. L. *J. Am. Chem. Soc.* **1979**, *101*, 3801.

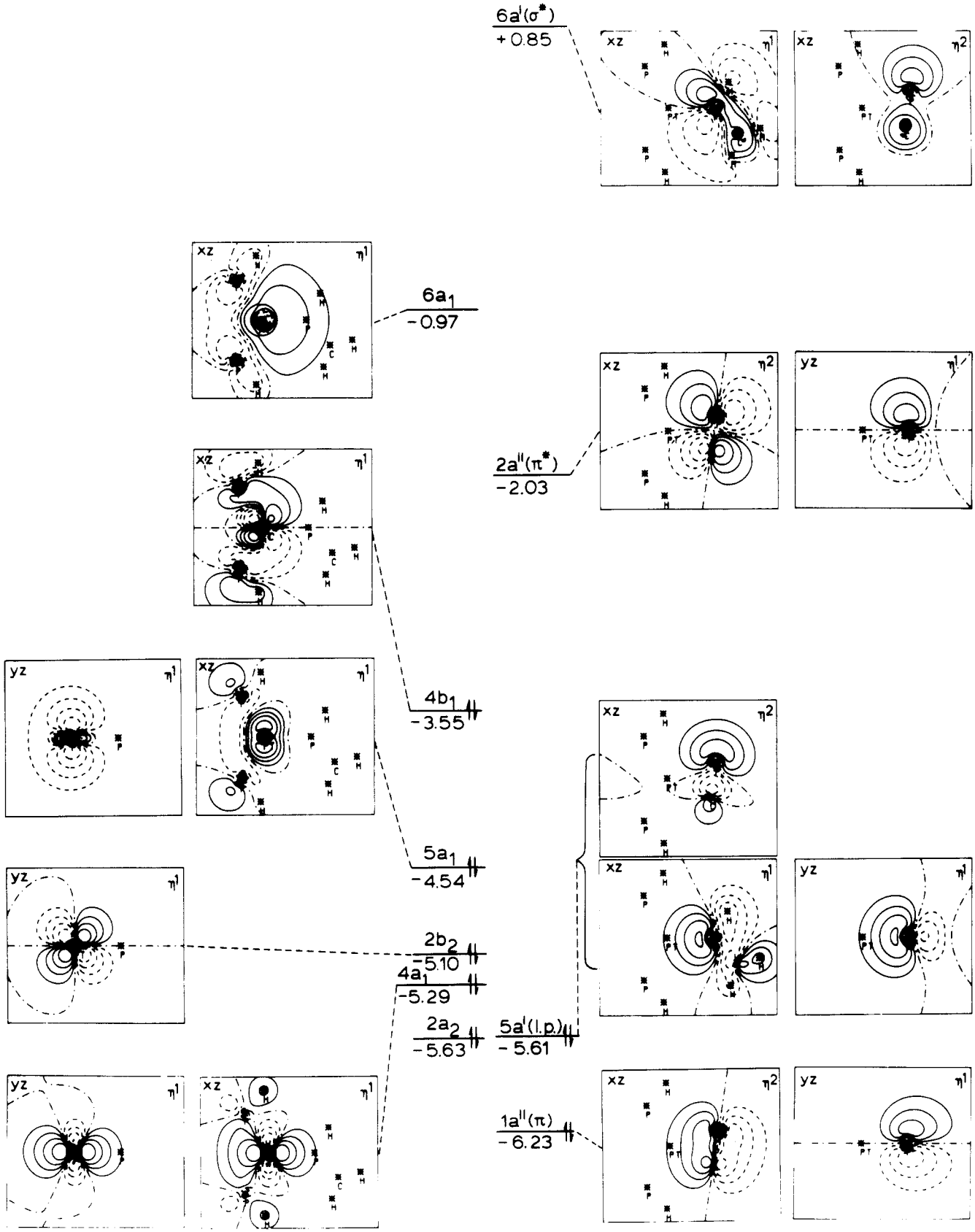

Figure 3. Orbital contour plots of relevant frontier orbitals of $Pt(PH_3)_2$ and $HP{=}CH_2$. Plots are in either the *xz* or *yz* plane (cf. **3a** and **3b**) for η^2_{xz}- or η^1_{xz}-coordination, respectively. The plane of the drawing is specified in the upper left corner and the coordination mode in the upper right corner. All nuclei in the plane of the drawing are indicated. Contour values are at 0.0, ±0.02, ±0.05, ±0.10, ±0.20, and ±0.50 $(e{\cdot}bohr^{-3})^{0.5}$.

electronic interaction energies and the overlap repulsion. The steric contribution is difficult to calculate and would probably not be very meaningful for **1** as we are using model ligands for **3** that are much smaller.

Considering first the population data of $Pt(PH_3)_2$, we note that the $4a_1$ orbital ("d_{z^2}") has considerably less than 2.0 electrons, notably in η^1-coordination. This is caused by strong overlap repulsion of d_{z^2} with occupied $HP{=}CH_2$

Table IV. One-Electron Energies of Free $Pt(PH_3)_2$ and $HP{=}CH_2$ and Gross Orbital Populations in Various Coordination Modes

orbital	type	orbital energy, eV	pop. electrons $\eta^2{}_{xz}$	$\eta^1{}_{xz}$	$\eta^1{}_{yz}$
		$Pt(PH_3)_2$			
$1a_1$	PH_3	−15.87	2.000	1.999	2.000
$2a_1$	PH_3	−9.67	1.998	1.999	2.000
$3a_1$	PH_3 lp	−7.89	1.992	1.999	2.001
$4a_1$	Pt d_{z^2}	−5.29	1.941	1.874	1.884
$5a_1$	Pt $d_{x^2-y^2}$	−4.54	1.970	1.985	1.970
$6a_1$	dsp hybrid	−0.97	0.279	0.339	0.351
$7\text{-}10a_1$			0.038	0.047	0.046
$1b_1$	PH_3	−15.75	1.999	1.999	2.000
$2b_1$	PH_3	−9.53	1.993	1.996	1.998
$3b_1$	PH_3	−7.61	1.981	1.991	1.993
$4b_1$	Pt d_{xz}	−3.55	1.496	1.786	1.712
$5\text{-}9b_1$		0.46	0.012	0.004	0.006
$1b_2$	PH_3	−9.86	1.999	2.000	2.000
$2b_2$	Pt d_{yz}	−5.10	1.969	1.864	1.905
$3\text{-}5b_2$			0.023	0.016	0.007
$1a_2$	PH_3	−9.85	2.000	2.000	2.000
$2a_2$	Pt d_{xy}	−5.63	1.994	1.995	1.995
$3\text{-}4a_2$			0.005	0.002	0.003
		$HP{=}CH_2$			
1a′	2s + 2s	−17.65	1.959	2.007	2.007
2a′	2s − 2s	−13.18	1.998	1.991	1.992
3a′	p_y, H	−10.50	1.991	1.996	1.996
4a′	p_σ, H	−9.11	1.997	1.984	1.980
5a′	P lp	−5.61	1.978	1.723	1.708
6a′	σ*	+0.85	0.014	0.142	0.062
7-11a′			0.045	0.121	0.073
1a″	π	−6.23	1.788	1.985	2.003
2a″	π*	−2.03	0.505	0.115	0.255
3a″			0.017	0.024	0.036

orbitals, which leads to rehybridization in the $Pt(PH_3)_2$ fragment to alleviate the repulsion. The fact that the decrease in d_{z^2} population is larger in η^1-coordination is in agreement with the stronger polarization expected from the larger d_{z^2}–lp overlap (0.193 in η^1) than d_{z^2}–π overlap (0.131 in η^2). The $Pt(PH_3)_2$ $6a_1$ orbital (dsp hybrid) clearly acts as as σ-acceptor. More charge is donated into $6a_1$ in the η^1-coordination (~0.35 e) than in η^2-coordination (0.28 e), in agreement with the larger overlap with lp (0.38) than with the $HP{=}CH_2$ π-orbital (0.28) and with the higher energy of the lp orbital. The electronic charge in the high-lying virtuals of $Pt(PH_3)_2$ reflects small charge transfers from $HP{=}CH_2$ and polarization of $Pt(PH_3)_2$ itself. In the B_1 symmetry, we observe a large reduction of the d_{xz} population, particularly in the η^2-coordination. This fits in with the expected π-back-bonding ability of d_{xz}. The overlap of π* with d_{xz} is larger in η^2-coordination (0.25) than in $\eta^1{}_{yz}$-coordination (0.20), which is reflected in the d_{xz} population. We note that also in $\eta^1{}_{xz}$-coordination, there is a considerable reduction of d_{xz} population, although there is virtually no overlap of d_{xz} with π* when $HP{=}CH_2$ is in the PPtP (i.e., xz) plane ($\eta^1{}_{xz}$). The σ* of $HP{=}CH_2$, however, has a significant overlap with d_{xz} (0.22!), and we find a population of 0.14 e in σ* in $\eta^1{}_{xz}$-coordination. We conclude that d_{xz} is always important for π-back-donation, although the DCD π-bonding is clearly the strongest. In B_2 symmetry we have the d_{yz}, which is less active than d_{xz}, in agreement with earlier findings,[16b,18,19] and with its lower energy and more contracted appearance in the contour plots (Figure 3). In $\eta^1{}_{xz}$-coordination, d_{yz} can interact with the π*, which leads to a noticeable reduction in d_{yz} population. It is evident, however, that the d_{xz} is more important, and the π-interaction alone would clearly favor DCD bonding and would cause a preference for $\eta^1{}_{yz}$ among the η^1-coordinations. In the A_2 symmetry, we see the expected inertness of d_{xy} reflected in the populations of 2.0 e for all coordination modes.

Turning now to the population data of $HP{=}CH_2$, we find the picture of the previous paragraph confirmed. The lp orbital (5a′) acts as a strong σ donor in the η^1-coordination modes, and the π-orbital does so, if somewhat less, in the η^2-coordination modes. The lp → $6a_1$ (dsp) donation is about equally strong in $\eta^1{}_{xz}$ and $\eta^1{}_{yz}$, thus not leading to directional preference. It is to be noted that there is a sizable population in the virtuals of A′ symmetry. This is partly due to metal → $HP{=}CH_2$ back-donation (cf. the d_{xz} → σ*-back-donation in $\eta^1{}_{xz}$) but also to polarization of the $HP{=}CH_2$ ligand. In the A″ symmetry we find the reduction in population of the π-orbital due to π → $6a_1$ (dsp) donation in η^2-coordination and the π*-population due to back-donation. This π*-population is very large (0.5 e) in η^2-coordination, which is indicative of the strength of the π-bond in the DCD bonding. In the η^1-coordination, there is considerably less π*-population for the $\eta^1{}_{xz}$ mode, as d_{yz} is less suited for back-donation.

We finally consider the energy terms given in Table VI in the light of the population data discussed above. We repeat that these energies may only be used for comparisons, to infer trends rather than absolute bond energies. First we wish to compare the $\eta^1{}_{xz}$- and $\eta^1{}_{yz}$-coordinations. In the A′ symmetry the lp orbital has considerable exchange repulsion with the occupied d_{z^2} and $d_{x^2-y^2}$ in both coordinations (overlaps of lp with d_{z^2} and $d_{x^2-y^2}$ are 0.193 and 0.144, respectively, in $\eta^1{}_{xz}$). The total overlap repulsion in A′ symmetry is slightly larger (2.5 kcal/mol) in $\eta^1{}_{xz}$. (The absolute values of the overlap repulsion terms are quite large. The electrostatic interaction is in general of the same order but of opposite sign.) In the A″ symmetry, the occupied π-orbital also has a repulsive interaction, in $\eta^1{}_{xz}$ with d_{yz} and in $\eta^1{}_{yz}$ with d_{xz} (overlaps 0.085 and 0.124, respectively). Due to the larger extension of d_{xz} in space and therefore larger overlap with the π-orbital, the A″ repulsion is larger in $\eta^1{}_{yz}$ by ~6 kcal/mol. The net effect (A′ + A″) is more repulsion (~4 kcal/mol) for $\eta^1{}_{yz}$.

Considering the attractive electronic interaction (HOMO/LUMO) terms, we have in A′ symmetry for both $\eta^1{}_{xz}$ and $\eta^1{}_{yz}$ the lp → $6a_1$ (dsp hybrid) donor bond, prob-

Table V. Overlaps of Selected $Pt(PH_3)_2$ Orbitals with Frontier Orbitals of $HP{=}CH_2$ in Various Coordination Modes

	$HP{=}CH_2$										
	$\eta^2{}_{xz}$			$\eta^1{}_{xz}$				$\eta^1{}_{yz}$			
$Pt(PH_3)_2$	π	π*	lp	π	π*	lp	σ*	π	π*	lp	σ*
$4a_1$ (d_{z^2})	0.131	−0.004	0.005	0	0	0.193	−0.053	0	0	0.195	−0.001
$5a_1$ ($d_{x^2-y^2}$)	−0.115	−0.024	−0.016	0	0	−0.144	0.045	0	0	−0.129	0.061
$6a_1$ (dsp)	0.279	0.055	0.118	0	0	0.380	−0.146	0	0	0.383	−0.145
$2b_2$ (d_{yz})	−0.004	−0.009	0.050	0.085	0.138	0	0	0	0	−0.017	0.159
$4b_1$ (d_{xz})	0.002	0.254	0.059	0	0	−0.025	0.223	0.124	0.196	0	0
$2a_2$ (d_{xy})	0.002	0.004	−0.044	0.008	0.017	0	0	0.008	0.017	0	0

Table VI. Selected Contributions to the $Pt(PH_3)_2$-HP=CH_2 Interaction Energy (kcal/mol)[a]

	η^2_{xz}	η^1_{xz}	η^1_{yz}
electronic interactn			
A′		−35 ($lp \rightarrow 6a_1$) ($\sigma^* \leftarrow d_{xz}$)	−31 ($lp \rightarrow 6a_1$) ($\sigma^* \leftarrow d_{yz}$)
A″		−11 ($\pi^* \leftarrow d_{yz}$)	−19 ($\pi^* \leftarrow d_{xz}$)
total	−95	−46	−50
exchange repulsn			
A′		+310 ($lp \leftrightarrow d_{z^2}$)	307.5 ($lp \leftrightarrow d_{z^2}$)
A″		7 ($\pi \leftrightarrow d_{yz}$)	13 ($\pi \leftrightarrow d_{xz}$)
total	+333	317	321

[a] Orbital interactions mainly responsible for individual terms are given in parentheses.

ably about equally strong in both cases. The back-bonding from d_{xz} (in η^1_{xz}) or d_{yz} (in η^1_{yz}) into the σ^* orbital is stronger for d_{xz} (see the populations in Table IV) due to the more favorable spatial characteristics and energy of d_{xz}. The total A′ energy is therefore larger for η^1_{xz} by ~4 kcal/mol. In the A″ symmetry, where we have the back-bonding of either d_{xz} (in η^1_{yz}) or d_{yz} (in η^1_{xz}) into the π^*, the d_{xz} acts stronger again and η^1_{yz} is more stable by ~8 kcal/mol. Taking all effects together (repulsion + attractive interactions) we find an almost perfect balance for the relative disadvantages and advantages of η^1_{xz} and η^1_{yz}. It is therefore not possible to predict one geometry or the other, as the total steric repulsion will be the decisive factor in the actual situation with bulky ligands such as in **1a**.

Next we compare the η^2- and η^1-coordination. As there is no symmetry in the η^2-coordination mode, we do not get separate contributions to the overlap repulsion and HOMO–LUMO interaction energies. We note that the total overlap repulsion in η^2 is 15 kcal/mol higher than with η^1-coordination. The main contribution to the overlap repulsion comes from the π-orbital with d_{z^2} and $d_{x^2-y^2}$ (overlaps 0.131 and 0.115 e). These overlaps are smaller than those of the lp orbital with d_{z^2} and $d_{x^2-y^2}$ in η^1-coordination. That the overlap repulsion is still considerably larger for η^2-coordination is probably due to the fact that it leads to more small but nonnegligible overlaps between occupied orbitals on the two fragments. This is intuitively plausible since in the η^1-coordination the =CH_2 end of the ligand bends away from the $Pt(PH_3)_2$ fragment. It is also confirmed by a detailed examination of all the overlaps (in η^2-mode, e.g., even the lp has overlaps of 0.016, 0.059, 0.050, 0.044 e with $d_{x^2-y^2}$, d_{xz}, d_{yz}, and d_{xy}). All these repulsive interactions add up to a relatively large overlap repulsion. This is, however, more than compensated by the strong bonds formed in the η^2-mode. We have already noted the large $d_{xz} \rightarrow \pi^*$ back-donation (0.505 e, instead of 0.255 e $d_{xz} \rightarrow \pi^*$ in η^1_{yz} and 0.115 e $d_{yz} \rightarrow \pi^*$ in η^1_{xz}). The σ-donation ($\pi \rightarrow 6a_1$) is also significant: 0.212 e out of π. The σ-bond is here probably less strong than in η^1-coordination, as the lp donates more electrons (0.28 e instead of 0.21 e), because it is higher in energy and has a better overlap with $6a_1$ than the π orbital (0.38 vs. 0.28). For σ- and π-bond together, however, we find a much larger stabilization energy (cf. Table VI) in the η^2-mode (95 kcal/mol vs. ~50 kcal/mol for η^1). This completely outweighs the larger repulsion in the η^2-mode. Our calculations thus suggest the η^2-coordination to be the most favorable one as far as orbital interactions are concerned. It is not to be expected that the electrostatic part of the steric repulsion, which we have not available, would reverse this order.

In view of the large back-bonding into π^* that we find in the η^2-coordination, a considerable lengthening of the P=C bond is to be expected. Our assumed P=C bond length of 1.65 Å, taken from an X-ray analysis of the η^1-coordinated **1a** is thus probably too short. This of course does not invalidate our conclusion with respect to the preference for η^2-coordination, but rather strengthens it.

Conclusion

Both experimental evidence and theoretical analysis underline the high versatility and unique ability of phosphaalkenes to function in either of two very general and important coordination modes. On the one hand, we find the synergistic σ-donative, π-bonding end-on coordination (η^1), e.g., **1a** or **3a**; a typical example of this type of bonding is CO, with the interesting difference that with CO, the π-bond makes the more important contribution,[20] whereas in **3a**, the σ-bond appears to be stronger. The second coordination mode of phosphaalkenes is the synergistic σ-donor, π-back-bonding side-on mode (η^2, "Dewar–Chatt–Duncanson"), typically exemplified by ethylene; for the alkenes and phosphaalkenes, the π-bond predominates.

In the model system $(PH_3)_2Pt$·HP=CH_2, theory predicts η^2-coordination to be favored by enthalpy over η^1-coordination because the effect of π-back-donation (π^* in $\eta^2 \gg \pi^*$ in η^1) overcompensates that of σ-donation (lone pair in $\eta^1 > \pi$ in η^2). However, it is conceivable that in phosphaalkenes bulkier than HP=CH_2, steric effects may overrule the subtle balance between the two bonding mechanisms.

The experimentally encountered situation in complex **1**, with the rather bulky **2** as a phosphaalkene ligand, still follows the trend predicted by theory for the simple model: the η^2-coordinated species **1b** is favored by enthalpy (ΔH = 4 kcal/mol^{-1}) over the η^1-coordinated species **1a**; at higher temperatures (above 0 °C), the situation is reversed due to entropy effects (ΔS = 15 cal·mol^{-1}·K^{-1}). As far as we are aware, this is the first case of such an equilibrium between the two coordination modes that is both close enough and kinetically accessible to make it directly observable.

Experiments are under way to illustrate the role of steric factors in either the P_2Pt fragment or the phosphaalkene ligand in shifting the position of this equilibrium.[24]

Experimental Section

The solid-state high-resolution ^{31}P NMR spectra were recorded at room temperature with a home-built spectrometer system. The spectrometer is equipped for cross-polarization and magic-angle spinning (CP MAS) NMR.[21] The resonance frequencies in the magnetic field of 4.2 T are 72.87 MHz for ^{31}P and 180.00 MHz for ^1H. The radio frequency magnetic field strengths used produced 90° pulses of 10 μs.

The powdered sample was contained in a Delrin rotor,[22] which was rotated at high speed (~4 kHz) around an axis inclined at the "magic" angle of 54.7° with respect to the magnetic field direction. The ^{31}P magnetization was prepared by matched $^{31}P\{^1H\}$ cross-polarization with a contact time of 5 ms, after which the ^{31}P free induction decay was measured in the presence of high power proton decoupling.[21] The proton spin temperature was alternated in successive sweeps to suppress artefacts in the spectra.[23] Approximately 20 000 sweeps were collected, from

(20) Ziegler, T.; Rauk, A. *Inorg. Chem.* **1979**, *18*, 1755.
(21) (a) Pines, A.; Gibby, M. G.; Waugh, J. S. *J. Chem. Phys.* **1973**, *59*, 569. (b) Schaefer, J.; Stejskal, E. O. *J. Am. Chem. Soc.* **1976**, *98*, 1031.
(22) Van Dijk, P. A. S.; Schut, W.; Van Os, J. W. M.; Menger, E. M.; Veeman, W. S. *J. Phys. E: Sci. Instrum.* **1980**, *13*, 1309.
(23) Stejskal, E. O.; Schaefer, J. *J. Magn. Reson.* **1975**, *18*, 560.
(24) **Note added in proof**: Dr. J. F. Nixon has informed us that he has independently investigated the solid-state ^{31}P NMR spectrum of **1a** and has reached similar results and conclusions.

which the spectra were obtained by Fourier transform.

Solution spectra were recorded on a Bruker WM-250 spectrometer ($^{31}P\{^1H\}$, $^{195}Pt\{^1H\}$).

[Mesityl(diphenylmethylene)phosphine]bis(triphenylphosphine)platinum(0) (1). Under argon, a solution of mesityl(diphenylmethylene)phosphine (**2**, 0.593 g, 1.88 mmol) in toluene (4 mL) was added to a suspension of $[Pt(PPh_3)_2C_2H_4]$ (1.39 g, 1.86 mmol) in toluene (5 mL). The dark red solution was stirred for 30 min at room temperature. On addition of pentane (100 mL), a red precipitate formed; it was filtered off, washed three times with pentane (10 mL), and dried in vacuo for 30 min; **1** was obtained as red crystals: mp 194–199 °C; 1.66 g, 86%, ^{31}P NMR, see Table I; ^{195}Pt NMR, see Table II; mass spectrum (FD), m/z 1035 (M^+·; isotopic pattern expected for **1**). Anal. Calcd for $C_{58}H_{51}P_3Pt$: C, 67.23; H, 4.96; P, 8.97. Found: C, 66.41; H, 5.27; P, 8.41.

Registry No. 1a, 80737-43-5; **1b**, 89934-21-4; **3a**, 92011-25-1; **3b**, 92011-26-2; $[Pt(PPh_3)_2C_2H_4]$, 12120-15-9; $Pt(PH_3)_2$, 76830-85-8; $HP{=}CH_2$, 61183-53-7.

Redox Properties of Bis[(η^5-cyclopentadienyl)dinitrosylchromium] and Related Complexes[1]

Peter Legzdins* and Berend Wassink

Department of Chemistry, The University of British Columbia, Vancouver, British Columbia, Canada V6T 1Y6

Received May 31, 1984

Cyclic voltammetry studies and bulk electrolyses at controlled potentials establish that $[CpCr(NO)_2]_2$ (Cp = η^5-C_5H_5) undergoes the following principal transformations in CH_2Cl_2 or CH_3CN when electrons are either removed from or added to it. Oxidation of the nitrosyl dimer is an irreversible two-electron process and affords $CpCr(NO)_2^+$ which in CH_3CN exists as $[CpCr(NO)_2(CH_3CN)]^+$. Upon reduction, the cation incorporates one electron and converts to the $CpCr(NO)_2$· radical that then reverts to $[CpCr(NO)_2]_2$. Reduction of the nitrosyl dimer is a reversible, one-electron process that results in the formation of the bimetallic radical anion $[CpCr(NO)_2]_2^-$·. This redox behavior of $[CpCr(NO)_2]_2$ is opposite to that exhibited under similar conditions by its isoelectronic carbonyl analogue, $[CpFe(CO)_2]_2$, which retains its bimetallic nature upon oxidation (initially a reversible, one-electron process) and undergoes scission upon reduction (an irreversible, two-electron process). On a preparative scale, these electron-transfer reactions of $[CpCr(NO)_2]_2$ are best effected with either HBF_4·OMe_2 in CH_2Cl_2 as the oxidant or $CpFe(\eta^6\text{-}C_6Me_6)$ in Et_2O as the reductant. The thermally stable oxidation product $CpCr(NO)_2^+$ is unisolable as such from CH_2Cl_2 but may be derivatized to $CpCr(NO)_2Cl$ in situ. The reduction product, $[CpFe(\eta^6\text{-}C_6Me_6)]^+$-$[\{CpCr(NO)_2\}_2]^-$·, however, is isolable from Et_2O, and its spectroscopic properties indicate substantial delocalization of the additional electron density in the radical anion onto the NO ligands. Electrochemical transfer of two electrons to $[CpCr(NO)_2]_2$ in CH_2Cl_2 does not result in the formation of the still unknown $[CpCr(NO)_2]^-$ anion but rather affords only low yields of green $Cp_2Cr_2(NO)_3(NH_2)$ and orange $[CpCr(NO)(NH_2)]_2$ as the principal nitrosyl-containing products. In contrast to the dinitrosyl dimer, the structurally similar $Cp_2Cr_2(NO)_3(NH_2)$ undergoes one-electron reduction more reluctantly and is apparently stabilized against cleavage upon electron removal by virtue of the presence of the better electron-donating μ-NH_2 group. Finally, one-electron reduction of $CpCr(NO)_2Cl$ effected electrochemically does not produce $[CpCr(NO)_2]_2$.

Introduction

During previous investigations[2-6] we have demonstrated that $[CpCr(NO)_2]_2$ (Cp = η^5-C_5H_5) generally exhibits markedly different chemistry than its isoelectronic and isostructural carbonyl analogue, $[CpFe(CO)_2]_2$. For instance, treatment of the two dimers with HBF_4·OMe_2 in CH_2Cl_2 results in the following conversions:[6]

$$[CpCr(NO)_2]_2 + 2HBF_4\cdot OMe_2 \xrightarrow{CH_2Cl_2} 2CpCr(NO)_2BF_4 + H_2 + 2OMe_2 \quad (1)$$

oxidative cleavage

$$[CpFe(CO)_2]_2 + HBF_4\cdot OMe_2 \xrightarrow{CH_2Cl_2} [\{CpFe(CO)_2\}_2H]BF_4 + OMe_2 \quad (2)$$

protonation

Furthermore, our preliminary electrochemical studies established that under identical experimental conditions the nitrosyl dimer undergoes oxidation at a more positive potential. Consequently, we could conclude that the differing chemical behavior summarized in reactions 1 and 2 is not simply a manifestation of the intrinsically differing tendencies of the two dimers to undergo oxidation but rather probably reflects the relative stabilities of analogous intermediate complexes.[6] We have now completed a more detailed study of the redox properties of $[CpCr(NO)_2]_2$ and some related complexes with a view to gaining further insight into the factors responsible for their characteristic chemical behavior and wish to report our observations herein.

Experimental Section

All reactions and subsequent manipulations involving organometallic reagents were performed under anaerobic and an-

(1) Organometallic Nitrosyl Chemistry. 21. For part 20 see: Legzdins, P.; Martin, D. T. *Organometallics* **1983**, *2*, 1785.
(2) Kolthammer, B. W. S.; Legzdins, P. *J. Chem. Soc., Dalton Trans.* **1978**, 31.
(3) Kolthammer, B. W. S.; Legzdins, P.; Martin, D. T. *Tetrahedron Lett.* **1978**, 323.
(4) Hames, B. W.; Legzdins, P.; Oxley, J. C. *Inorg. Chem.* **1980**, *19*, 1565.
(5) Ball, R. G.; Hames, B. W.; Legzdins, P.; Trotter, J. *Inorg. Chem.* **1980**, *19*, 3626.
(6) Legzdins, P.; Martin, D. T.; Nurse, C. R.; Wassink, B. *Organometallics* **1983**, *2*, 1238.

0276-7333/84/2303-1811$01.50/0